



Microvascular invasion and grading in hepatocellular carcinoma: correlation with major and ancillary features according to LIRADS

Vincenza Granata¹ · Roberta Fusco¹ · Sergio Venanzio Setola¹ · Carmine Picone¹ · Paolo Vallone¹ · Andrea Belli² · Paola Incollingo² · Vittorio Albino² · Fabiana Tatangelo³ · Francesco Izzo² · Antonella Petrillo¹

Published online: 14 May 2019
© Springer Science+Business Media, LLC, part of Springer Nature 2019

Abstract

Purpose To assess major and ancillary parameters that could be correlated with Microvascular Invasion (MIV) and with histologic grade of HCC.

Materials and methods In this retrospective study, we assessed 62 patients (14 women–48 men; mean age, 63 years; range 38–80 years) that underwent hepatic resection for HCC. All patients were subject to Multidetector computed tomography (MDCT); 40 to Magnetic Resonance (MR) study. The radiologist assessed major and ancillary features according to LIRADS (v. 2018) and reported any radiological accessory findings if detected.

Results No major feature showed statistically significant differences and correlation with grading. Mean ADC value was correlated with grading and with MIV status. No major feature was correlated to MIV; progressive contrast enhancement and satellite nodules showed statistically different percentages with respect to the presence of MIV, so as at the monivariate correlation analysis, satellite nodules were correlated with the presence of MIV. At multivariate regression analysis, no factor proved to be strong predictors of grading while progressive contrast enhancement and satellite nodules were significantly associated with the MIV.

Conclusion Mean ADC value is correlated to HCC grading and MIV status. Progressive contrast enhancement and the presence of satellite nodules are correlated to MIV status.

Keywords Hepatocellular carcinoma · Microvascular invasion · Histological grading · Multidetector computed tomography · Magnetic resonance imaging

Introduction

Liver resection (LR) and orthotopic liver transplantation (OLT) are considered the standard of care of hepatocellular carcinoma (HCC) [1–3]. However, the high recurrence rate is a major problematic issue for hepatic resection with regard to achieving cure and long-term survival, because the tumor

recurrence rate exceeds 60% at 5 years even in patients with small tumors [4]. Microvascular invasion (MVI), defined as microscopically detected tumor thrombi within small tumor or peritumoral vessels, today, is considered a major risk factor of recurrence and survival in patients with HCCs after curative resection [5]. In addition, macrovascular and microvascular invasion have been shown to increase the risk of tumor recurrence after liver transplantation. The value of MVI is particularly stressed after OLT, because the long-term result in these patients is not satisfactory [6–9]. Conversely, for patients referred for LR, the rule of MVI is not widely accepted. In fact, there is no well-defined correlation between overall and disease-free survival (DFS) with MVI [10]. Nevertheless, the assessment of MVI could be important in establishing the different phases of therapy, as the choice between LR or ablation therapies [11–13], or to identify a personalized post-treatment follow-up [14, 15]. Therefore, it is important to predict the presence of MVI

✉ Roberta Fusco
r.fusco@istitutotumori.na.it

¹ Radiology Division, Istituto Nazionale Tumori IRCCS Fondazione Pascale – IRCCS di Napoli, 80131 Naples, Italy

² Hepatobiliary Surgical Oncology Division, Istituto Nazionale Tumori IRCCS Fondazione Pascale – IRCCS di Napoli, 80131 Naples, Italy

³ Pathology Diagnostic Division, Istituto Nazionale Tumori IRCCS Fondazione Pascale – IRCCS di Napoli, 80131 Naples, Italy

before hepatic resection for helping physicians in determining treatment strategies. Conversely to macrovascular invasion, conventional imaging techniques have been ineffective in detecting MVI since MVI is a microscopic parameter and the criteria for preoperative diagnosis of MIV are not well established [16, 17]. Also, HCC histologic grade is an important predictive factor for recurrence and survival after hepatic resection and transplantation: poorly differentiated HCCs are associated to worse survival in comparison to well- and moderately differentiated HCCs [18]. The possibility that imaging features can correlate to histologic grade to select the therapeutic strategy would be of great value in helping to direct proper management of HCC [5, 18]. The accurate detection of histologic grade of HCC is thought to be a main parameter in planning the therapeutic approach [5, 18].

The purpose of this retrospective study is to assess morphological parameters that could be correlated with MIV and with histologic grade of HCC.

Materials and methods

Study population

Our institutional review board approved this retrospective study, and the requirement for patient informed consent was waived. We searched the surgical database at our institution from May 2012 to September 2018 and selected 84 patients with suspected HCC, who underwent hepatic resection. The inclusion criteria for the study population were as follows: (a) patients who had pathologically proven HCC; (b) patients who had undergone MR imaging and liver MDCT with less than a 1-month interval between imaging modalities; (c) patients who had less than a 1-month interval between

imaging and pathologic diagnosis; and (d) availability of diagnostic quality pictures of the cut sections of the resected specimens in patients who underwent surgical resection for matching of imaging and pathology findings. The exclusion criteria were as follows: (a) divergence between the imaging-based diagnosis and the pathologically confirmed diagnosis, (b) no available MR or MDCT images.

In total, 84 patients with HCC confirmed at pathology fulfilled the inclusion criteria during the study period. Among them, 22 patients were excluded for the following reasons: (a) four patients had no available MR or MDCT images and (b) in 18 patients the final diagnosis did not show HCC.

Finally, 62 patients [16 women–46 men; mean age, 63 years; range 38–78 years) comprised our study population. Characteristics of the 62 patients are summarized in Table 1.

Lesion confirmation: reference standard

All original pathological samples were reviewed by one experienced hepatic pathologist (F.T.). Lesions were confirmed histopathologically as hepatic tumors according to the tumor classification of the World Health Organization and the grading were defined according to the grading system of Edmondson–Steiner. The HCC component was defined as trabecular, solid sheet, or pseudoacinar arrangements with interspersed sinusoids. For each specimen, hepatocellular differentiation was confirmed with immunohistochemical stains characteristic of hepatocyte differentiation (Hepatocyte-Paraffin-1).

Follow-up

The follow-up programed for all patients was CEUS at first month and MDCT every 3 months for the first post-operative

Table 1 Characteristics of the 62 selected patients

Description	Numbers (%) / Range
Gender	Men 46 (74.2%) Women 16 (25.8%)
Age	63 years; range 38–78 years
Number of hepatic nodules	
Single nodule	62 (100%)
Multiple nodules	/
Nodule size (mm)	mean size 53.0 mm; range 12–190 mm
Risk factor for HCC	
Chronic hepatitis B HBV-related liver cirrhosis	32 (51.6%)
Chronic hepatitis C HCV-related liver cirrhosis	29 (46.7)
Alcoholic liver cirrhosis	/
Child–Pugh classification	
A	62 (100%)
B	

year. If a new liver nodule was detected at imaging, patients underwent MRI examination.

MDCT and MR examinations

All patients were subject to MDCT and 40 to MR study.

MDCT protocol

MDCT was performed with a 64-detector row scanner (Optima 660, GE Healthcare, United States). MDCT scanning parameters were 120 kVp, 100–470 mAs (NI 16.36), 2.5-mm slice thickness, and table speed 0.984/1 mm/rotation. Scans were carried out including a region encompassing the liver from diaphragm to iliac crests. Liver protocol examinations were composed of quadruple phases, including the unenhanced, arterial, portal venous, and equilibrium phases. CT images were obtained after injection of 120 mL of a non-ionic contrast medium (iomeprol, Iomeron 400, Bracco, Milan, Italy) at a rate of 3.0–4.0 mL/s by using an automatic power injector (Empower CTA, E-Z-EM Inc., New York, United States). Image acquisition in the arterial phase which was initiated 19 s after attenuation in the descending aorta reached 100 HU, as measured with the bolus tracking method; in the portal venous phase, images were acquired 33 s after the arterial phase; in the equilibrium phase, images were acquired 180 s after administration of contrast media.

MR imaging protocol

MR imaging was performed by using a 1.5 T scanner (Magnetom Symphony, with Total Imaging Matrix Package, Siemens, Erlangen, Germany) with an 8-element body coil and a phased array coil. Our routine liver MR imaging protocol consisted of a breath-hold fat-saturated and not fat-saturated T2-weighted turbo spin-echo sequence, an in- and opposed-phase T1-weighted gradient-echo sequence, dynamic imaging with a fat-saturated T1-weighted gradient-echo sequence, and diffusion-weighted imaging. Diffusion-weighted imaging (DWI) was obtained with planar echo-pulse sequence [b values 0, 50, 100, 200, 400, 600, and 800 s/mm²]. A non-specific agent, the Gd-BT-DO3A (Gadovist, Bayer Schering Pharma, Germany), was employed. All patients received 0.1 mL/kg of Gd-BT-DO3A by means of a power injector (Spectris Solaris[®] EP MR, MEDRAD Inc., Indianola, IA, USA), at an infusion rate of 2 mL/s followed by a 30-mL saline flush. Arterial phase images were acquired 7 s after contrast material arrival at the thoracic aorta by using an MR fluoroscopic monitoring system. Thereafter, portal venous phase and equilibrium phase were obtained 60 s and 3 min after contrast material administration, respectively. Detailed

information regarding the MR imaging parameters is summarized in manuscript [18].

Image analysis

For each patient, MDCT and MR images were independently and blindly evaluated in random order within and between three radiologists (V.G., S.V.S., A.P.; 10, 15, and 20 years of experience in abdominal imaging). A consensus evaluation was performed when there was disagreement between the readers. The readers were blinded to previous radiological examination, pathologic results, and history of previous treatment but were aware that the patients had cirrhosis and thus were at higher risk for HCC. To reduce recall bias, all three readers maintained an interval of more than 2 weeks between interpretation sessions of MR and MDCT images.

Each radiologist was asked to identify the presence of lesion that was considered to be detectable if the nodule had attenuation or signal intensity that differed from that of the surrounding liver parenchyma. Thereafter, they reported the presence of the HCC assessing major and ancillary features according to LIRADS v. 2018 [19]; also the radiologists reported any radiological accessory findings if detected.

Readers assessed and recorded the following parameters: greatest nodule diameter, attenuation at unenhanced CT, signal intensity on T1- and T2-weighted images, DWI and ADC map, vascular hyperenhancement pattern during arterial phase, wash-out appearance during portal phase, vascular enhancement during equilibrium or late phases [13]. The signal intensity of the lesions was categorized subjectively as isointense, hypointense, or hyperintense compared to the surrounding liver parenchyma. We assessed the signal on DWI sequences and measured the ADC of each lesion. The diffusion-weighted signal decay was analyzed using the mono-exponential model, according to the equation $ADC = (\ln(S_0/S_b))/b$, where S_b is the signal intensity with diffusion weighting b and S_0 is the non-diffusion-weighted signal intensity. This analysis is based on ROI using median value of single voxel signals for each b value. ROIs for the tumor were manually drawn to include such hyperintense voxels on image at b value 800 s/mm². Median diffusion parameters of ROI were used as representative values for each lesion. No motion correction algorithm was used but ROIs were drawn taking care to exclude areas in which movement artifacts or blurring caused voxel misalignments.

We analyzed the enhancement pattern during arterial, portal, and equilibrium or late phase and described it as homogeneous, heterogeneous, or progressive. We described the capsule appearance or pseudocapsule, defined as a peripheral rim of smooth hyperenhancement in the portal or delayed phase, as complete or partial. In addition, the researches were asked to report the presence of other imaging findings if present.

Statistical analyses

Each variable was summarized by frequencies and percentages. Chi-square test was performed to assess statistically significant difference between percentage values. Monovariate correlation analysis by means of the Rho Spearman's Coefficient was performed to determine the factors (non-rim arterial phase hyperenhancement, wash-out, pseudocapsule, hyperintensity in T2, restricted signal in DWI, progressive contrast enhancement, satellite nodules) that are associated with grading and MIV. Mann–Whitney non-parametric test was used to compare a continuous variable among 2 or more groups. A multivariate logistic regression analysis was performed to determine the factors that were associated with the grading equal to 3 and with the MIV. Sensitivity, specificity, positive predictive value, negative predictive value, and accuracy were calculated for each factors with respect to grading and the presence of vascular invasion.

A p value < 0.05 was considered statistically significant.

All statistical analysis was performed with SPSS for Windows (Version 23.0; SPSS Inc, Chicago, Ill).

Results

We assessed 62 patients that underwent surgical resection with preoperative diagnosis of HCC. Twelve patients were classified as G3 (19.4%), 1 as G1 (1.6%), and 49 as G2 (79.0%) according to the grading system of Edmondson–Steiner (ES) [21].

According to the surgical procedure, nine patients were subject to lobectomy, 2 mesohepatectomy, 27 bi-segmentectomy, and 24 segmentectomy (6 for VII, 1 for I, 2 for II, 2 for III, 6 for IV, 5 for V, and 2 for VI hepatic segment).

Pathological features

In 18 HCC reported with microvascular invasion, 9 lesions with MIV were G2 and 9 with MIV were G3.

Patient survival

To date all patients are alive. We found a new hepatic lesion (mean time 6.8 months) in six patients (9.7%); four patients were MIV (22.2% of MIV patients). During follow-up (mean time 14 months), in seven patients (4 were G3 and 3 were G2; 3 with MIV) we found metastases (mean time 13 months). In one case the lesion was pulmonary, in two cases were mesenteric, and in one case was bone (Fig. 1) and in 3 cases we found nodal metastases.



Fig. 1 A 63-year-old man with HCC. MDCT study shows costal metastasis

Imaging features

All lesions were detected and analyzed by readers. The consensus in the assessment of the nodules was 100%. The mean size was 53.0 mm; range 12–190 mm.

Table 2 reports the frequencies for each imaging feature with respect to grading and MIV. No factor showed statistically significant differences and correlation with grading (Table 3). The progressive contrast enhancement and satellite nodules showed statistically different percentages with respect to the presence of MIV (p value = 0.03 and 0.002 at Chi-square test, respectively; see Table 2). Moreover, at the monovariate correlation analysis (Table 3), satellite nodules was correlated with the presence of MIV (p value < 0.05). A statistically significant difference was detected between ADC median value between the grading ≤ 2 (mean ADC $2149 \times 10^{-3} \text{ mm}^2/\text{s}$) (Fig. 2) and grading = 3 ($1715 \times 10^{-3} \text{ mm}^2/\text{s}$). A statistically significant difference was detected between ADC median value in the groups without ($2138 \times 10^{-3} \text{ mm}^2/\text{s}$) and with MIV ($1801 \times 10^{-3} \text{ mm}^2/\text{s}$). Table 4 reports diagnostic performance for each factors with respect to grading and respect to the presence of MIV (Fig. 3). Progressive contrast enhancement and the presence of satellite nodules had an accuracy according to grading equal to 74% and 77%, respectively. The presence of satellite nodules reached an accuracy of 79% according to the presence of MIV.

Table 5 shows the finding of the multivariate logistic regression analysis. Statistically significant p value (≤ 0.05)

Table 2 Imaging features in study population according to grading and according to vascular invasion

Imaging features in study population according to grading	Grading ≤ 2 (number) <i>N</i> = 50	Grading ≤ 2 (%)	Grading 3 (number) <i>N</i> = 12	Grading 3 (%)	<i>p</i> value*
Non-rim arterial phase hyperenhancement					
Yes	31	62.0	8	66.7	0.72
Inhomogeneous	17	34.0	3	25.0	
No	2	4.0	1	8.3	
Wash-out					
Yes	35	70.0	8	66.7	0.92
Inhomogeneous	10	20.0	3	25.0	
No	5	10.0	1	8.3	
Pseudocapsule					
Yes	27	54.0	6	50.0	0.84
Alone	1	2.0	0	0.0	
No	22	44.0	6	50.0	
Hyperintensity in T2					
Yes	22	78.6	8	66.7	0.69
No	2	7.1	2	16.7	
Inhomogeneous	4	14.3	2	16.7	
Restricted signal in DWI					
Yes	28	100.0	12	100.0	–
Progressive contrast enhancement					
Yes	8	16.0	4	33.3	0.17
Satellite nodules					
Yes	6	12.0	4	33.3	0.07
Imaging features in study population according to Vascular Invasion	Without Vascular Invasion (number) <i>N</i> = 44	Without Vascular Invasion (%)	With Vascular Invasion (number) <i>N</i> = 18	With Vascular Invasion (%)	<i>p</i> value*
Non-rim arterial phase hyperenhancement					
Yes	29	67.4	10	52.6	0.52
Inhomogeneous	12	27.9	8	42.1	
No	2	4.7	1	5.3	
Wash-out					
Yes	31	72.1	12	63.2	0.08
Inhomogeneous	6	14.0	7	36.8	
No	6	14.0	0	0.0	
Pseudocapsule					
Yes	19	44.2	9	47.4	0.68
Alone	0	0.0	1	5.3	
No	24	55.8	9	47.4	
Hyperintensity in T2					
Yes	22	88.0	12	80.0	0.79
No	1	4.0	2	13.3	
Inhomogeneous	2	8.0	1	6.7	
Restricted signal in DWI					
Yes	25	100.0	15	100.0	–
Progressive contrast enhancement					
Yes	7	16.3	5	26.3	0.03
Satellite nodules					
Yes	2	4.7	8	42.1	0.002

*Chi-square test

Table 3 Correlation between imaging features

		Wash-in	Wash-out	Pseudocapsule	T2 hyperintensity	Progressive contrast enhancement	Presence of satellite nodules	Grading
Non-rim arterial phase hyperenhancement	Spearman's Correlation coefficient	1.000	0.440**	0.481**	0.857**	-0.405**	-0.246	-0.002
	<i>p</i> value		0.000	0.000	0.000	0.001	0.054	0.985
Wash_out	Spearman's Correlation coefficient	0.440**	1.000	0.413**	0.599**	-0.469**	-0.136	0.041
	<i>p</i> value	0.000		0.001	0.003	0.000	0.292	0.749
Pseudocapsule	Spearman's Correlation coefficient	0.481**	0.413**	1.000	0.733**	-0.370**	-0.213	-0.003
	<i>p</i> value	0.000	0.001		0.000	0.003	0.097	0.984
T2 hyperintensity	Spearman's correlation coefficient	0.857**	0.599**	0.733**	1.000	-0.488*	-0.177	-0.122
	<i>p</i> value	0.000	0.003	0.000		0.018	0.418	0.579
Progressive contrast enhancement	Spearman's correlation coefficient	-0.405**	-0.469**	-0.370**	-0.488*	1.000	0.562**	0.181
	<i>p</i> value	0.001	0.000	0.003	0.018		0.000	0.160
Presence of satellite nodules	Spearman's correlation coefficient	-0.246	-0.136	-0.213	-0.177	0.562**	1.000	0.232
	<i>p</i> value	0.054	0.292	0.097	0.418	0.000		0.069
Grading	Spearman's correlation coefficient	-0.002	0.041	-0.003	-0.122	0.181	0.232	1.000
	<i>p</i> value	0.985	0.749	0.984	0.579	0.160	0.069	

Correlation between imaging features and vascular invasion

		Wash-in	Wash-out	Pseudocapsule	T2 hyperintensity	Progressive contrast enhancement	Satellite nodules	Vascular invasion
Non-rim arterial phase hyperenhancement	Spearman's correlation coefficient	1.000	0.440**	0.481**	0.857**	-0.405**	-0.246	-0.135
	<i>p</i> value		0.000	0.000	0.000	0.001	0.054	0.295
Wash_out	Spearman's correlation coefficient	0.440**	1.000	0.413**	0.599**	-0.469**	-0.136	-0.037
	<i>p</i> value	0.000		0.001	0.003	0.000	0.292	0.773
Pseudocapsule	Spearman's correlation coefficient	0.481**	0.413**	1.000	0.733**	-0.370**	-0.213	-0.056
	<i>p</i> value	0.000	0.001		0.000	0.003	0.097	0.665
T2 hyperintensity	Spearman's correlation coefficient	0.857**	0.599**	0.733**	1.000	-0.488*	-0.177	-0.037
	<i>p</i> value	0.000	0.003	0.000		0.018	0.418	0.869
Progressive contrast enhancement	Spearman's correlation coefficient	-0.405**	-0.469**	-0.370**	-0.488*	1.000	0.562**	0.117
	<i>p</i> value							

Table 3 (continued)

Correlation between imaging features and vascular invasion

		Wash-in	Wash-out	Pseudocapsule	T2 hyperintensity	Progressive contrast enhancement	Satellite nodules	Vascular invasion
Presence of satellite nodules	<i>p</i> value	0.001	0.000	0.003	0.018		0.000	0.365
	Spearman's correlation coefficient	−0.246	−0.136	−0.213	−0.177	0.562**	1.000	0.469**
	<i>p</i> value	0.054	0.292	0.097	0.418	0.000		0.000
Vascular invasion	Spearman's correlation coefficient	−0.135	−0.037	−0.056	−0.037	0.117	0.469**	1.000
	<i>p</i> value	0.295	0.773	0.665	0.869	0.365	0.000	

*Significant for test at one tail

**Significant for test at two tails

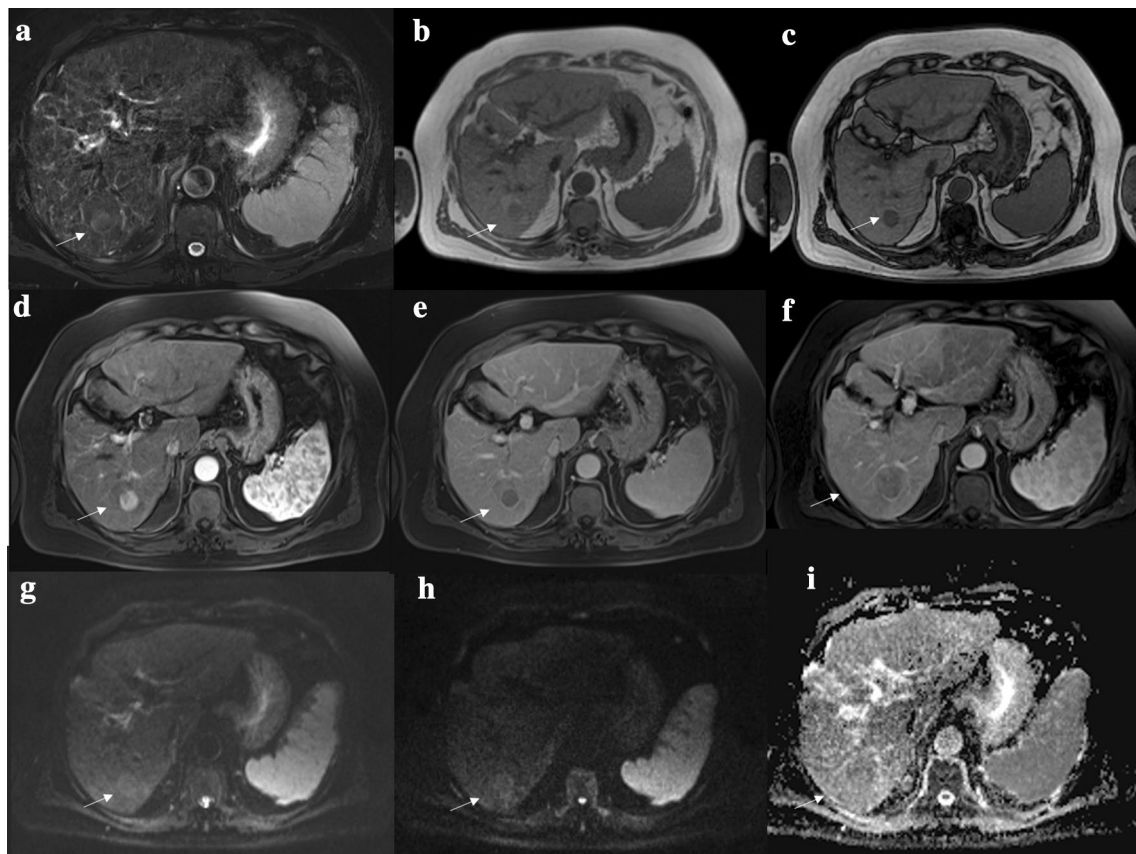
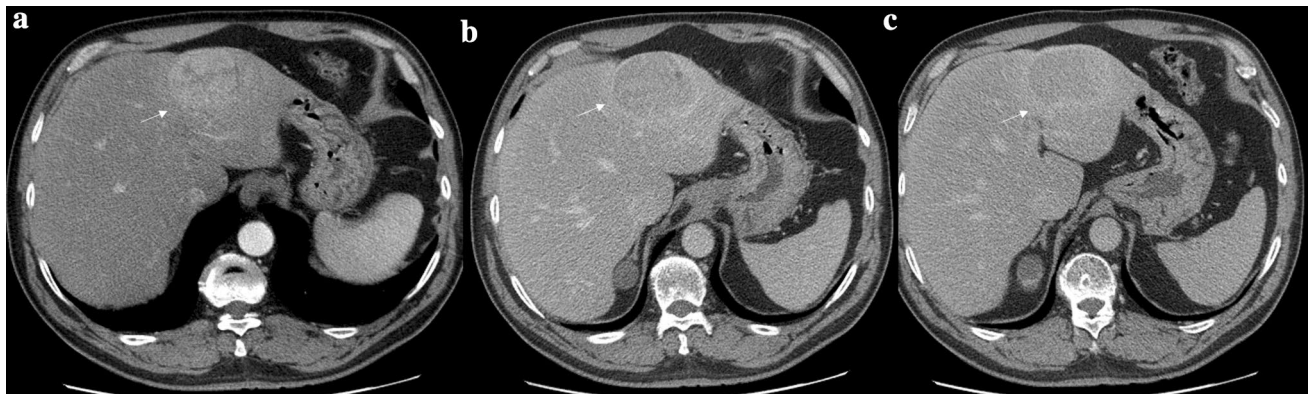


Fig. 2 A 58-year-old woman with G2 HCC on VII hepatic segment. MRI study. The lesion shows inhomogeneous hyperintense signal (arrow) in T2-W sequence (a). In T1-W in-out phase sequence (b and c) the lesion is hypointense (arrow). The lesion shows hypervascular

appearance (arrow) during arterial phase (d) with wash-out appearance (arrow) and capsule appearance during portal phase (e) and late phase (f) of contrast study. The lesion shows restricted diffusion (arrow) in DWI sequences (g, h and i)

Table 4 Diagnostic performance of imaging features in terms of sensitivity (SEN), specificity (SPEC), positive predictive value (PPV), negative predictive value (NPV), and accuracy (ACC)

	SEN	SPEC	PPV	NPV	ACC
According to grading					
Non-rim arterial phase hyperenhancement	0.67	0.38	0.21	0.83	0.44
Wash-out	0.92	0.10	0.20	0.83	0.26
Pseudocapsule	0.00	1.00	–	0.81	0.81
Progressive contrast enhancement	0.33	0.84	0.33	0.84	0.74
Presence of satellite nodules	0.33	0.88	0.40	0.85	0.77
T2 hyperintensity	0.33	0.68	0.20	0.81	0.61
ADC	0.17	0.90	0.29	0.82	0.76
According to MIV					
Non-rim arterial phase hyperenhancement	0.00	1.00	–	0.69	0.69
Wash-out	1.00	0.14	0.34	1.00	0.40
Pseudocapsule	0.00	1.00	–	0.69	0.69
Progressive contrast enhancement	0.26	0.84	0.42	0.72	0.66
Presence of satellite nodules	0.42	0.95	0.80	0.79	0.79
T2 hyperintensity	0.00	1.00	–	0.69	0.69
ADC	0.00	1.00	–	0.69	0.69

**Fig. 3** A 71-year-old man with HCC on II hepatic segment. MDCT study. The nodule shows inhomogeneous hypervascular appearance (arrow) during arterial phase (a), with inhomogeneous wash-out

appearance (arrow) and not complete capsule appearance (arrow) during portal and late phase of contrast study (b and c)

was highlighted in bold. No factor proved to be strong predictors of grading while progressive contrast enhancement and the presence of satellite nodules (Fig. 4) were significantly associated with the MIV.

Discussion

We assessed 62 patients that underwent surgical resection with preoperative diagnosis of HCC. Twelve patients were classified as G3 (19.4%), 1 as G1 (1.6%), and 49 as G2 (79.0%). In 18 HCC reported with microvascular invasion, 9 were G2, and 9 were G3, so that no statistical analysis was performed.

No vascular parameters showed statistically significant differences and correlation with grading. The presence of

the specific vascular profile characterized by contrast arterial uptake followed by wash-out in the venous phases has allowed defining the non-invasive diagnostic criteria for HCC [20]. However, these criteria show a sensitivity rate of 50–60% in lesion smaller than 2 cm [20] and are correlated to the hemodynamic changes in nodule during hepatocarcinogenesis [21]. The typical uptake of contrast medium during arterial phase is due to neoangiogenesis, sinusoidal capillarization, and the increase of unpaired arteries, changes that take place during carcinogenesis from high-grade dysplastic nodule to classic HCC. During this process, the main drainage of vessels goes from veins to sinusoids and then to portal veins [21]. This drainage was well assessed in the late phase of contrast studies. Histological examination revealed continuity between a tumor sinusoid and a portal venule in the pseudocapsule (HCC with

Table 5 Multivariate regression analysis

	Coefficients	Standard error	Significance value	<i>p</i> value
According to grading				
Non-rim arterial phase hyperenhancement	0.10	0.11	0.39	0.74
Wash-out	0.01	0.10	0.90	
Pseudocapsule	0.00	0.07	0.99	
Progressive contrast enhancement	0.12	0.19	0.54	
Presence of satellite nodules	0.22	0.18	0.22	
T2 hyperintensity	−0.10	0.13	0.46	
ADC	0.14	0.19	0.46	
According to MIV				
Non-rim arterial phase hyperenhancement	−0.05	0.12	0.67	0.01
Wash-out	−0.01	0.10	0.91	
Pseudocapsule	0.01	0.07	0.90	
Progressive contrast enhancement	−0.28	0.20	0.02	
Presence of satellite nodules	0.74	0.19	0.00	
T2 hyperintensity	0.04	0.14	0.79	
ADC	−0.06	0.19	0.74	

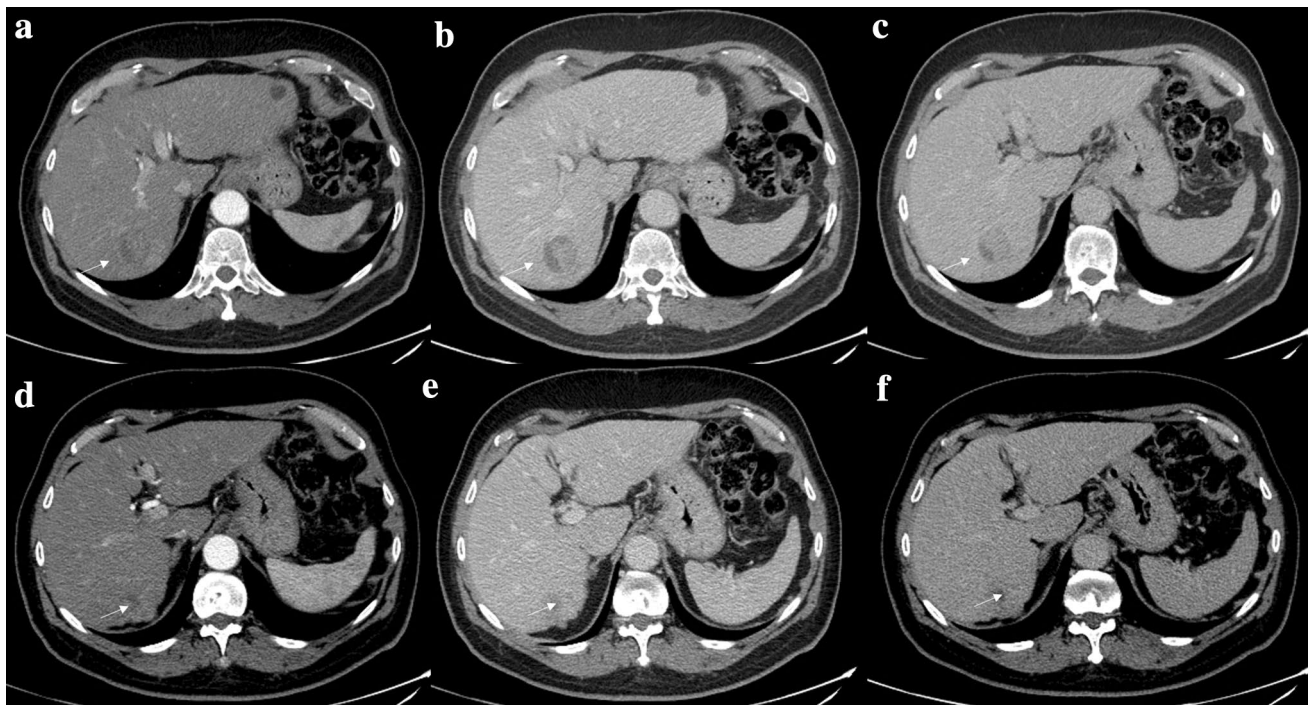


Fig. 4 A 58-year-old woman with HCC on VII hepatic segment. MDCT study. The nodule shows inhomogeneous hypervascular appearance (arrow) during arterial phase (a), with progressive contrast enhancement (arrow), without capsule appearance (arrow) dur-

ing portal and late phase of contrast study (b and c). Above the HCC, arrow shows satellite nodule, more evident in portal (e) and late phase (f) than in arterial phase (d) of contrast study

pseudocapsule appearance) or surrounding hepatic sinusoids (HCC without pseudocapsule). According to the hypothesis that these hemodynamic changes should correlate with the histological grade of HCC, our results show that there are no statistically significant differences and correlation between

grading and arterial hyperenhancement, between grading and portal wash-out, and between grading and capsule appearance. Our results are similar to the results of Schelhorn et al. [22]; these researches assessed the imaging features extracted by combined Gd-EOB-DTPA and gadobutrol

liver-MRI to predict HCC grading, showing that a significant correlation with grading was not found for either the combined dynamic information of all gadobutrol phases or all the Gd-EOB-DTPA phases. No correlation with grading was found for a combination of arterial and hepatocellular phase in Gd-EOB-DTPA MRI, a combination of both arterial phases (gadobutrol and Gd-EOB-DTPA) with the Gd-EOB-DTPA hepatocellular phase, or a combination of all available gadobutrol and Gd-EOB-DTPA phases. For all gadobutrol information (dynamic phases and morphology) and for all Gd-EOB-DTPA information, no correlation with grading was found [22]. Conversely, we found a statistically significant difference between ADC median value in the grading ≤ 2 (mean ADC $2149 \times 10^{-3} \text{ mm}^2/\text{s}$) and grading = 3 ($1715 \times 10^{-3} \text{ mm}^2/\text{s}$). These results are similar to the results of our previous study in which we showed that ADC and IVIM parameters should have a role in predicting the histological grade of HCC [18]. In fact, we found a good correlation between ADC, fp (perfusion fraction), and Dt (tissue diffusivity) and tumoral grading. ROC analyses demonstrated that an ADC value of $2.11 \times 10^{-3} \text{ mm}^2/\text{s}$, an fp value of 47%, and an Dt value of $0.94 \times 10^{-3} \text{ mm}^2/\text{s}$ were the most accurate cut-off levels, with a sensitivity and specificity for ADC of 100 and 100%, for fp of 100 and 89%, and for Dt of 100 and 74%, respectively [18]. Nakanishi et al. showed not only the utility of DWI for histological grading, but also that ADC should be used as a preoperative prediction of early recurrence [23]. Chen et al., in a meta-analysis, found that for differentiating well-differentiated lesions from higher grades, DWI showed a low sensitivity (54%), high specificity (90%), and an excellent diagnostic performance. Conversely, in differentiating poorly differentiated lesion from lower grades, the sensitivity was 84%, the specificity 48%, showing a moderately high diagnostic performance [24]. Nasu et al. demonstrated no correlation between histological grade and ADC, while they found that Signal Intensity (SI) of the HCC increased in higher grade [25]. The major limit of DWI and IVIM parameters to identify the histological grade of HCC, as suggested by Ichikawa et al. [26], is correlated to the fitting model used to extract functional data, thus the fitting would be robust even though some errors might have occurred during image acquisition [26]. Contrary to Nasu [25], in our study, we found no correlation between SI on T2-W sequences and histological grade of HCC. According to LIRADS, T2-W hyperintensity is an ancillary feature. Park et al. [27] showed that dysplastic nodules and HCCs cannot be distinguished on the basis of SI, since their signal intensities are similar on T1-W and T2-W sequences. However, dysplastic nodules are almost never hyperintense on T2-W sequences, early HCCs are mostly isointense on T2-W sequences, while higher grade (moderately or poorly) of HCC is associated with high SI on T2-W images, although the SI may also be related with

tumor vascularity and peliotic changes [27]. The major limit of our analysis is that it is a qualitative analysis. Conversely to us, Wu et al. investigated the value of MRI-based radiomics signatures for the preoperative prediction of HCC grade [28]. They evaluated 170 confirmed HCC. The radiomics features of tumors based on both T1-W imaging and T2-W imaging were extracted, and radiomics signatures were generated using the least absolute shrinkage and selection operator (LASSO) logistic regression model. The predicted values of pathological HCC grades using radiomics signatures, clinical factors (including age, sex, tumor size, alpha fetoprotein (AFP) level, history of hepatitis, hepatocirrhosis, portal vein tumor thrombosis, portal hypertension, and pseudocapsule), and the combined models were assessed. They demonstrated that radiomics signatures could successfully categorize high-grade and low-grade HCC cases ($p < 0.05$) in both the training and test datasets. Regarding the performances of clinical factors, radiomics signatures, and the combined clinical and radiomics signature (from the combined T1-W and T2-W images) models for HCC grading prediction, the areas under the curve (AUCs) were 0.600, 0.742, and 0.800 in the test datasets, respectively. Both the AFP level and radiomics signature were independent predictors of HCC grade ($p < 0.05$) [28].

MVI has drawn worldwide attention in recent years, since it is indicative of early invasion of tumor cells into the tumor vessels. In our study population, we showed that there was no difference between patients with and without MIV about recurrence or metastases from HCC during the follow-up. The presence of MVI should be recognized based on microscopy, since it is beyond the imaging resolution and cannot be directly visualized with current imaging technology; however, several imaging features may be predictive of MVI [10, 29, 30]. In our study group, we found MIV in 18 HCC (29.0%); among them, 9 lesions with MIV were G2 and 9 were G3. The mean size was 36.1 mm (range 20 to 70 mm). Our results differ from Portolani et al. which reported that HCCs with MVI are generally of large size ($> 5 \text{ cm}$), with satellite nodules, a high value of AFP, and poor grading [10]. The unique finding that makes our study similar to Portolani is the presence of satellite nodules. According to our results, the satellite nodules and progressive contrast enhancement showed statistically different percentages with respect to the presence of MIV ($p \text{ value} = 0.03$ and 0.002 at Chi-square test, respectively). Moreover, at the monivariate correlation analysis, the presence of satellite nodules was correlated with the presence of MIV ($p \text{ value} < 0.05$). Progressive contrast enhancement and the presence of satellite nodules had an accuracy according to grading equal to 74% and 77%, respectively. The presence of satellite nodules reached an accuracy of 79% according to the presence of MIV. At multivariate logistic regression analysis, no factor proved to be strong predictors of grading while progressive contrast enhancement and the presence of

satellite nodules were significantly associated with the MIV. When we analyzed vascular pattern of HCC with and without MIV, we found that no parameters showed statistically significant differences and correlation with MIV, such as the capsule appearance. These data are different to those reported in literature. Several researches reported that the presence of non-smooth tumor margins, no or incomplete capsule, intratumoral arteries, and large tumor size detected on contrast-enhanced dynamic CT and MRI are associated with an increased risk for MVI [29–34]. According to our results, Chandarana et al. showed that tumor multifocality at imaging was the only variable that was significantly correlated with the presence of MIV [33]. No other clinical, pathologic, or imaging features were useful in significantly predicting MIV [33]. In our study, we found that histopathologic tumor grade was not significantly correlated with MIV, since 9 lesions with MIV were G2 and 9 lesions were G3. These results are similar to those by Chandarana et al. and in contradiction to prior studies showing that tumor grade is an independent predictor of MIV [35, 36]. Regarding DWI, we found a statistically significant difference between ADC median value without ($2138 \times 10^{-3} \text{ mm}^2/\text{s}$) and with MIV ($1801 \times 10^{-3} \text{ mm}^2/\text{s}$). These results are similar to those reported by previous studies, showing that DWI is an interesting tool in the assessment of MIV during preoperative phase [37–40]. Limits of our analysis are related to the fact that in this retrospective study we assessed only conventional DWI; our future prospectives are to investigate the role of IVIM and Kurtosis DWI. In fact, as demonstrated by Li et al., histogram analysis of IVIM based on whole tumor volume can be useful for predicting MVI. The 5th percentile of D was the most useful value to predict MVI of HCC [41]. Also Zhao et al. investigated the usefulness of IVIM in predicting MVI in HCC. Preoperative IVIM DW imaging and Gd-EOB-DTPA-enhanced MRI of 51 patients were analyzed. The ADC, D (the true diffusion coefficient), D^* (the pseudodiffusion coefficient) and f (the perfusion fraction), relative enhancement (RE); and radiological features were analyzed. Univariate analysis revealed that HCCs with MVI had a higher portion of an irregular tumor shape than HCCs without MVI. ADC, D value was significantly lower in HCCs with MVI. Multivariate analysis revealed that an irregular shape and D value $\leq 1.16 \times 10^{-3} \text{ mm}^2/\text{s}$ were independent predictors for MVI. Combining the two factors of an irregular shape and D value, a sensitivity of 94% and specificity of 64% for predicting MVI were obtained [16]. Wang et al. evaluated the role of diffusion kurtosis imaging (DKI) and conventional MR imaging findings including ADC and morphologic features for prediction of MVI. They assessed 84 patients with 92 histopathologically confirmed HCCs (40 MVI-positive lesions and 52 MVI-negative lesions). Univariate and multivariate logistic regression analyses were used to evaluate the relative value of these parameters as potential predictors of MVI. They showed that features significantly related to MVI at univariate analysis

were increased mean kurtosis value, decreased mean diffusivity value, ADC value, the presence of infiltrative border with irregular shape, and irregular circumferential enhancement. At multivariate analysis, mean kurtosis value as well as irregular circumferential enhancement were independent risk factors for MVI [40].

Regarding T2-W SI, we found no correlation between SI on T2-W sequences and MIV. The limit of this evaluation is the qualitative analysis; in fact, we think that a radiomics analysis should give significant results on MVI status.

There are several limitations to our study. First, the sample size by a single-center experience; second, this is a retrospective study with a possible selection bias; third, the study is defective of functional assessment of IVIM, Kurtosis, and radiomics features. Our future prospective is to assess the rule of these functional parameters in evaluating correlation with grading and MIV status.

Conclusions

MIV and grading are two independent features that are considered major risk factors of recurrence and survival in patients with HCCs after curative resection or OLT. Although MIV cannot be directly visualized with current imaging technology, however, several imaging features may be predictive of MVI and of grading. In our study, no major feature shows statistically significant differences and correlation with grading. Mean ADC value is correlated with grading and with MIV status. Regarding MIV, the progressive contrast enhancement and the presence of satellite nodules show statistically different percentages with respect to the presence of MIV.

Acknowledgements The authors are grateful to Alessandra Trocino, librarian at the National Cancer Institute of Naples, Italy. Moreover, for the collaboration, authors are grateful to Assunta Zazzaro and Dr Ivano Rossi, TSRM at Radiology Division, “Istituto Nazionale Tumori IRCCS Fondazione Pascale – IRCCS di Napoli,” Naples, I-80131, Italy.

Compliance with ethical standards

Conflict of interest The authors have no conflict of interest to be disclosed. The authors confirm that the article is not under consideration for publication elsewhere. Each author has participated sufficiently in any submission to take public responsibility for its content.

References

1. Raza A, Sood GK. Hepatocellular carcinoma review: current treatment, and evidence-based medicine. *World J Gastroenterol*. 2014 Apr 21;20(15):4115–27.
2. Cascales-Campos P, Martinez-Insfran LA, Ramirez P, Ferreras D, Gonzalez-Sanchez MR, Sanchez-Bueno F, Robles R, Pons JA, Capel A, Parrilla P. Liver Transplantation in Patients With Hepatocellular Carcinoma Outside the Milan Criteria After Downstaging: Is It Worth It? *Transplant Proc*. 2018 Mar;50(2):591–594.

3. Yilmaz C, Karaca CA, Iakobadze Z, Farajov R, Kilic K, Doganay L, Kilic M. Factors Affecting Recurrence and Survival After Liver Transplantation for Hepatocellular Carcinoma. *Transplant Proc.* 2018 Dec;50(10):3571-3576.
4. Poon RT, Fan ST, Lo CM, et al. Long-term survival and pattern of recurrence after resection of small hepatocellular carcinoma in patients with preserved liver function: implications for a strategy of salvage transplantation. *Ann Surg* 2002; 235:373–82.
5. Granata V, Fusco R, Filice S, Catalano O, Piccirillo M, Palaia R, Izzo F, Petrillo A. The current role and future perspectives of functional parameters by diffusion weighted imaging in the assessment of histologic grade of HCC. *Infect Agent Cancer.* 2018 Jul 3; 13:23.
6. Esnaola NF, Lauwers GH, Mirza NQ et al (2002) Predictors of microvascular invasion in patients with hepatocellular carcinoma who are candidates for orthotopic liver transplantation. *J Gastrointest Surg* 6:224–232.
7. Mitsunobu M, Toyosaka A, Oriyama T et al (1996) Intrahepatic metastases in hepatocellular carcinoma: the role of the portal vein as an efferent vessel. *Clin Exp Metastasis* 14:520–529.
8. Pawlik TM, Delman KA, Vauthey JN et al (2005) Tumor size predicts vascular invasion and histologic grade: implication for selection of surgical treatment for hepatocellular carcinoma. *Liver Transpl* 11:1086–1092.
9. Piardi T, Gheza F, Ellero B et al (2012) Number and tumor size are not sufficient criteria to select patients for liver transplantation for hepatocellular carcinoma. *Ann Surg Oncol* 19:2020–2026.
10. Portolani N, Baiocchi GL, Molfino S, Benetti A, Gheza F, Giulini SM. Microvascular infiltration has limited clinical value for treatment and prognosis in hepatocellular carcinoma. *World J Surg.* 2014 Jul;38(7):1769-76.
11. Izzo F, Palaia R, Albino V, Amore A, di Giacomo R, Piccirillo M, Leongito M, Nasto A, Granata V, Petrillo A, Lastoria S. Hepatocellular carcinoma and liver metastases: clinical data on a new dual-lumen catheter kit for surgical sealant infusion to prevent perihepatic bleeding and dissemination of cancer cells following biopsy and loco-regional treatments. *Infect Agent Cancer.* 2015 Apr 10;10:11.
12. Roayaie S, Jibara G, Tabrizian P, Park JW, Yang J, Yan L, Schwartz M, Han G, Izzo F, Chen M, Blanc JF, Johnson P, Kudo M, Roberts LR, Sherman M. The role of hepatic resection in the treatment of hepatocellular cancer. *Hepatology.* 2015 Aug;62(2):440-51. <https://doi.org/10.1002/hep.27745>
13. Golfieri R, Bilbao JI, Carpanese L, Cianni R, Gasparini D, Ezziddin S, Paprotka PM, Fiore F, Cappelli A, Rodriguez M, Ettorre GM, Saltarelli A, Geatti O, Ahmadzadehfar H, Haug AR, Izzo F, Giampalma E, Sangro B, Pizzi G, Notarianni E, Vit A, Wilhelm K, Jakobs TF, Lastoria S; European Network on Radioembolization with Yttrium-90 Microspheres (ENRY) study collaborators. Comparison of the survival and tolerability of radioembolization in elderly vs. younger patients with unresectable hepatocellular carcinoma. *J Hepatol.* 2013 Oct;59(4):753-61.
14. Granata V, Petrillo M, Fusco R, Setola SV, de Lutio di Castelguidone E, Catalano O, Piccirillo M, Albino V, Izzo F, Petrillo A. Surveillance of HCC Patients after Liver RFA: Role of MRI with Hepatospecific Contrast versus Three-Phase CT Scan-Experience of High Volume Oncologic Institute. *Gastroenterol Res Pract.* 2013; 2013:469097.
15. Granata V, de Lutio di Castelguidone E, Fusco R, Catalano O, Piccirillo M, Palaia R, Izzo F, Gallipoli AD, Petrillo A. Irreversible electroporation of hepatocellular carcinoma: preliminary report on the diagnostic accuracy of magnetic resonance, computer tomography, and contrast-enhanced ultrasound in evaluation of the ablated area. *Radiol Med.* 2016 Feb;121(2):122-31.
16. Zhao W, Liu W, Liu H, Yi X, Hou J, Pei Y, Liu H, Feng D, Liu L, Li W. Preoperative prediction of microvascular invasion of hepatocellular carcinoma with IVIM diffusion-weighted MR imaging and Gd-EOB-DTPA-enhanced MR imaging. *PLoS One.* 2018 May 17;13(5): e0197488.
17. Zhao J, Li X, Zhang K, Yin X, Meng X, Han L, Zhang X. Prediction of microvascular invasion of hepatocellular carcinoma with preoperative diffusion-weighted imaging: A comparison of mean and minimum apparent diffusion coefficient values. *Medicine (Baltimore).* 2017 Aug;96(33):e7754.
18. Granata V, Fusco R, Catalano O, Guarino B, Granata F, Tatan-gelo F, Avallone A, Piccirillo M, Palaia R, Izzo F, Petrillo A. Intravoxel incoherent motion (IVIM) in diffusion-weighted imaging (DWI) for Hepatocellular carcinoma: correlation with histologic grade. *Oncotarget.* 2016 Nov 29;7(48):79357-79364.
19. The American College of Radiology website (<https://www.acr.org/Clinical-Resources/Reporting-and-Data-Systems/LI-RADS/CT-MRI-LI-RADS-v2018>).
20. Granata V, Fusco R, Avallone A, Catalano O, Filice F, Leongito M, Palaia R, Izzo F, Petrillo A. Major and ancillary magnetic resonance features of LI-RADS to assess HCC: an overview and update. *Infect Agent Cancer.* 2017 Apr 28; 12:23.
21. Matsui O, Kobayashi S, Sanada J, et al. Hepatocellular nodules in liver cirrhosis: hemodynamic evaluation (angiography-assisted CT) with special reference to multi-step hepatocarcinogenesis. *Abdom Imaging.* 2011;36(3):264–72.
22. Schelhorn J, Best J, Dechêne A, Göbel T, Bertram S, Lauenstein T, Kinner S. Evaluation of combined Gd-EOB-DTPA and gadobutrol magnetic resonance imaging for the prediction of hepatocellular carcinoma grading. *Acta Radiol.* 2016 Aug;57(8):932-8.
23. Nakanishi M, Chuma M, Hige S, Omatsu T, Yokoo H, Nakanishi K, Kamiyama T, Kubota K, Haga H, Matsuno Y, Onodera Y, Kato M, Asaka M. Relationship between diffusion-weighted magnetic resonance imaging and histological tumor grading of hepatocellular carcinoma. *Ann Surg Oncol.* 2012 Apr;19(4):1302-9. <https://doi.org/10.1245/s10434-011-2066-8>
24. Chen J, Wu M, Liu R, Li S, Gao R, Song B. Preoperative evaluation of the histological grade of hepatocellular carcinoma with diffusion-weighted imaging: a meta-analysis. *PLoS One.* 2015;10(2): e 0117661.
25. Nasu K, Kuroki Y, Tsukamoto T, et al. Diffusion-weighted imaging of surgically resected hepatocellular carcinoma: imaging characteristics and relationship among signal intensity, apparent diffusion coefficient, and histopathologic grade. *AJR Am J Roentgenol.* 2009; 193:438–44.
26. Ichikawa S, Motosugi U, Hernando D, Morisaka H, Enomoto N, Matsuda M, Onishi H. Histological grading of hepatocellular carcinomas with Intravoxel incoherent motion diffusion-weighted imaging: inconsistent results depending on the fitting method. *Magn Reson Med Sci.* 2017.
27. Park YN, Kim MJ. Hepatocarcinogenesis: imaging-pathologic correlation. *Abdom Imaging.* 2011;36:232–43.
28. Wu M, Tan H, Gao F, Hai J, Ning P, Chen J, Zhu S, Wang M, Dou S, Shi D. Predicting the grade of hepatocellular carcinoma based on non-contrast-enhanced MRI radiomics signature. *Eur Radiol.* 2018 Nov 7.
29. Chou CT, Chen RC, Lin WC, ko CJ, Chen CB, Chen yL. Prediction of microvascular invasion of hepatocellular carcinoma: preoperative CT and histopathologic correlation. *AJR Am J Roentgenol* 2014; 203: W253-W25.
30. Lim JH, Choi D, Park Ck, Lee WJ, Lim Hk. Encapsulated hepatocellular carcinoma: CT-pathologic correlations. *Eur Radiol* 2006; 16: 2326-2333.
31. ZhaoH,HuaY,DaiT,HeJ,TangM,FuX,MaoL,JinH,Qiu y. Development and validation of a novel predictive scoring model for microvascular invasion in patients with hepatocellular carcinoma. *Eur J Radiol* 2017; 88: 32-40.

32. Banerjee S, Wang DS, Kim HJ, Sirlin CB, Chan MG, Korn RL, Rutman AM, Siripongsakun S, Lu D, Imanbayev G, Kuo MD. A computed tomography radiogenomic biomarker predicts microvascular invasion and clinical outcomes in hepatocellular carcinoma. *Hepatology* 2015; 62: 792-800.
33. Chandarana H, Robinson E, Hajdu CH, Drozhinin L, Babb JS, Taouli B. Microvascular invasion in hepatocellular carcinoma: is it predictable with pretransplant MRI? *AJR Am J Roentgenol* 2011; 196: 1083-1089.
34. Kim H, Park MS, Choi Jy, Park yN, Kim MJ, Kim kS, Choi JS, Han kH, Kim E, Kim kW. Can microvessel invasion of hepatocellular carcinoma be predicted by pre-operative MRI? *Eur Radiol* 2009; 19: 1744-1751.
35. Kim BK, Han KH, Park YN, et al. Prediction of microvascular invasion before curative resection of hepatocellular carcinoma. *J Surg Oncol* 2008; 97:246–252.
36. Wayne JD, Lauwers GY, Ikai I, et al. Preoperative predictors of survival after resection of small hepatocellular carcinomas. *Ann Surg* 2002; 235: 722–730; discussion, 730–731.
37. Suh YJ, Kim MJ, Choi Jy, Park MS, Kim kW. Preoperative prediction of the microvascular invasion of hepatocellular carcinoma with diffusion-weighted imaging. *Liver Transpl* 2012; 18: 1171-1178.
38. Okamura S, Sumie S, Tonan T, Nakano M, Satani M, Shimose S, Shirono T, Iwamoto H, Aino H, Niizeki T, Tajiri N, Kuromatsu R, Okuda k, Nakashima O, Torimura T. Diffusion-weighted magnetic resonance imaging predicts malignant potential in small hepatocellular carcinoma. *Dig Liver Dis* 2016; 48: 945-952 [PMID: 27338850 <https://doi.org/10.1016/j.dld.2016.05.020>]
39. Xu P, Zeng M, Liu k, Shan y, Xu C, Lin J. Microvascular invasion in small hepatocellular carcinoma: is it predictable with preoperative diffusion-weighted imaging? *J Gastroenterol Hepatol* 2014; 29: 330-336.
40. Wang WT, Yang L, Yang ZX, Hu XX, Ding y, Yan X, Fu CX, Grimm R, Zeng MS, Rao SX. Assessment of Microvascular Invasion of Hepatocellular Carcinoma with Diffusion kurtosis Imaging. *Radiology* 2018; 286: 571-580.
41. Li H, Zhang J, Zheng Z, Guo Y, Chen M, Xie C, Zhang Z, Mei Y, Feng Y, Xu Y. Preoperative histogram analysis of intravoxel incoherent motion (IVIM) for predicting microvascular invasion in patients with single hepatocellular carcinoma. *Eur J Radiol*. 2018 Aug;105:65-71.

Publisher's Note Springer Nature remains neutral with regard to jurisdictional claims in published maps and institutional affiliations.